Nonequilibrium dynamics of free quantum-well excitons in time-resolved photoluminescence

C. Piermarocchi, F. Tassone, V. Savona, and A. Quattropani
Institut de Physique Théorique, Ecole Polytechnique Fédérale, CH-1015 Lausanne, Switzerland

P. Schwendimann
Defense Procurement and Technology Agency, System Analysis Division, 3003 Bern, Switzerland
(Received 13 November 1995; revised manuscript received 2 February 1996)

Scattering rates of quantum-well excitons by acoustic phonons are calculated using realistic deformation potentials for electrons and holes in structures based on GaAs. These rates are used in order to reproduce the exciton dynamics in a time-resolved photoluminescence experiment. Rise time and decay time of the luminescence signal are studied as a function of temperature and quantum-well size. It is found that the exciton distribution function reaches a stationary shape during the radiative recombination and shows strong deviations from the thermal distribution. As a consequence, the decay time is slower. A discussion of the dependence of these effects on the well width is given. [S0163-1829(96)01223-4]

I. INTRODUCTION

Energy relaxation in optical excitation processes in quantum wells (QW's) is a fundamental subject for the characterization of the time response of optical devices. In this framework, time-resolved photoluminescence (PL) experiments represent a reliable probe for the understanding of the microscopic dynamics. Theoretical investigations have been made to obtain a picture of the processes involved in these experiments and particular attention has been devoted to the study of the photoluminescence decay times.[1–3] On the other hand, the improvement of the microstructure growing techniques have recently allowed the study of the relaxation dynamics of free QW excitons in good quality samples.[3–6] In these samples, the PL decay times are linearly increasing with temperature. This result has been only qualitatively interpreted by the theoretical models.[1–3] In particular, the experiments show deviations from a linear behavior at low temperatures, and slopes steeper than those theoretically predicted at higher temperatures. An assumption common to all theoretical models is that phonon scattering rates between excitations at different energies are much larger than the radiative recombination rates in the range of temperature considered. Under this assumption, phonon scattering is fast enough to balance exciton recombination, and a Boltzmann-like distribution function of the exciton population results.

In this paper, we revisit this assumption. In particular, we want to take into account the perturbation produced by radiative decay on the Boltzmann-like distribution function. We solve rate equations for the exciton population in which the rates of scattering of free QW excitons by acoustic phonons and the radiative rates are calculated exactly. We find that even when phonon scattering rates are larger than radiative recombination rates, thermalization is not fully achieved for all excitons. The exciton distribution function deviates from a Boltzmann-like distribution mainly in the radiative zone. However, only indirect observation of this nonthermal distribution is possible, because only a tiny portion of the radiative zone is probed in the experiments.

In Sec. II, we describe our model of a time-resolved PL experiment, and we calculate the rates of phonon absorption and emission, as well as the radiative recombination rate for free QW excitons. The limits of validity of the model are discussed. In Sec. III, we introduce a rate equation model to obtain the time evolution of the exciton distribution function in the case of resonant and nonresonant excitation. Furthermore, we discuss the dynamics obtained from the solution of the rate equations and the corresponding time evolution of the PL signal. An exhaustive analysis of the temperature dependence of the rise time and of the decay time is given in Sec. IV. Here, we also present a simplified model showing how the deviations from the thermal distribution modify the luminescence decay times. We also investigate the dependence of the luminescence characteristic times on the quantum-well width. Finally, in Sec. V, we discuss the role of spin-flip scattering in the exciton dynamics.

II. MODEL OF A TIME-RESOLVED PHOTOLUMINESCENCE EXPERIMENT

In a time-resolved PL experiment, we have three different steps in the dynamics: the excitation of the system in which excitons are created, the relaxation toward the lowest exciton levels, and, finally, the radiative recombination. In this paper, we consider the dynamics within a single excitonic band [$1s$ heavy hole (HH) excitons]. Actually, also other higher levels, such as $2s$, $2p$, ... the continuum of HH exciton, the light hole, and eventually other subbands, contribute to the relaxation dynamics depending on the excitation conditions and temperature. In particular, the continuum of states is expected to be relevant, because of its high density of states. In fact, the dynamics inside the exciton continuum is very fast, as it has been experimentally well assessed.[7] It has been found that in this continuum the photoexcited carriers relax towards a hot distribution with typical relaxation times, which do not exceed few picoseconds. It has also been experimentally found[6] that, when the sample is excited near the light hole (LH) exciton level, the relaxation towards the bottom of HH exciton band slows down considerably. We restrict our discussion to QW's narrower than 120 Å, where

the LH level is well above the bottom of the continuum of the HH exciton, and to excitation energies far from the LH resonance. In this way, we can completely neglect the influence of the LH on the relaxation. In our model, the presence of the HH continuum of states is taken into account in the choice of the initial condition for the integration of the rate equations, as discussed below. The exciton excited states $2s$, $2p$, . . . in the two-dimensional (2D) case have a small binding energy and are close to the exciton continuum. Thus, their role in the dynamics cannot be distinguished from the role of the continuum. Finally, we consider here only free excitons, and we disregard the exciton trapping due to interface roughness and impurities. This assumption holds for the good quality samples currently used in the measurements.[3–6]

In the case of nonresonant PL, the excitation process is modeled assuming that the laser pulse excites high energy levels. The hot carriers created in this way relax toward the bottom of the exciton continuum (e-h pairs), and the time needed for this first relaxation is very short, as several experimental measurements have pointed out.[7] We investigate the dynamics of the system just after this first relaxation, assuming a hot distribution of the carriers in the continuum. The hot electrons and holes provide for the creation of excitons with large in-plane wave vector, mainly through a fast acoustic phonon emission. This process is nearly elastic at low temperature, because the acoustic phonon energy is negligible compared to the exciton binding energy. Exciton formation by emission of optical phonons may be completely neglected when excess energies in the excitation are smaller than the optical phonon energy. This energy is quite large in the polar materials considered, typically 36 meV in GaAs. Therefore, we assume that the excitons are created with a distribution function peaked at the edge of the exciton continuum. We will consider this distribution as the initial condition for the integration of the rate equations.

Excitons are created in contact with a thermal bath of phonons at a given lattice temperature and we assume the scattering by acoustic phonons as the only effective relaxation mechanism. This approximation holds for low excitonic density when we can neglect the effect due to the exciton-exciton and exciton-carrier scattering. The excitation densities n that we consider in our model are thus $n \ll a_B^{-2}$, and $n \ll \lambda^{-2}$, where a_B and λ, are the Bohr radius and the screening length of the Coulomb interaction in the sample; the upper limit densities correspond to about 10^{11}–10^{12} exc/cm^2. The exciton-acoustic phonon scattering originates from the deformation potential interaction,

$$U(r_e, r_h) = \Delta(r_e) a_e - \Delta(r_h) a_h, \tag{1}$$

where $\Delta(r_e)$ and $\Delta(r_h)$ are the relative deformations of the lattice induced by phonons at the points where the electron and the hole are located, and a_e and a_h are the deformation potentials experimentally measured. The exciton-phonon interaction results from the sum of the phonon-electron and phonon-hole interaction. For the deformation potentials, we use the GaAs bulk values $a_e = -7$ eV for electrons, and $a_h = 2.7$ eV for holes.[8,9] Equation (1) represents only the isotropic term, which is related to the longitudinal branch of acoustic phonons. Since GaAs is a polar material, piezoelectric scattering also occurs, but it provides a negligible contribution to the exciton dynamics.[10] At low temperature ($T \leqslant 100$ K), we can also neglect the scattering by optical phonons in the relaxation process, because they are not excited. The exciton-phonon Hamiltonian corresponding to the deformation potential interaction of Eq. (1) is given by

$$H_{\text{exc-ph}} = \sum_{q_z} \sum_{\mathbf{q},\mathbf{k},\mathbf{k}'} G(\mathbf{q}, q_z)\, \delta_{\mathbf{k}', \mathbf{k}+\mathbf{q}} (c_{\mathbf{q},q_z} - c^{\dagger}_{-\mathbf{q},q_z}) b^{\dagger}_{\mathbf{k}'} b_{\mathbf{k}}, \tag{2}$$

where $b^{\dagger}_{\mathbf{k}}$ ($b_{\mathbf{k}}$) is the creation (annihilation) operator of 2D excitons with the in-plane wave vector $\mathbf{k}$, and $c^{\dagger}_{\mathbf{q},q_z}$ ($c_{\mathbf{q},q_z}$) is the creation (annihilation) of 3D phonons with the wave vector $(\mathbf{q}, q_z)$ (z is the growth direction). Translational invariance along the QW plane implies the conservation of the in-plane momentum $\mathbf{k}$, as explicitly shown in Eq. (2) by the presence of the Kronecker δ function. The z component of the wave vector in not conserved and a sum over q_z appears in Eq. (2). The term $G(\mathbf{q}, q_z)$ contains all the parameters of the interaction and reads

$$G(\mathbf{q}, q_z) = i \sqrt{\frac{\hbar (|\mathbf{q}|^2 + q_z^2)^{1/2}}{2 \rho V u}} [a_e I_e^{\parallel}(|\mathbf{q}|) I_e^{\perp}(q_z) - a_h I_h^{\parallel}(|\mathbf{q}|) I_h^{\perp}(q_z)]. \tag{3}$$

Here, ρ and u are the density and the longitudinal sound velocity in GaAs, respectively, and V is the quantization volume. The terms $I^{\parallel}_{e(h)}(|\mathbf{q}|)$ and $I^{\perp}_{e(h)}(q_z)$ are the superposition integrals of the exciton envelope function with the phonon wave function (plane wave) in the in-plane and z directions, respectively. Using the exciton envelope function,

$$F(\boldsymbol{\rho}, z_e, z_h) = \sqrt{\frac{2}{\pi a_B^2}} e^{-|\boldsymbol{\rho}|/a_B} f_e(z_e) f_h(z_h), \tag{4}$$

where $\boldsymbol{\rho}$ is the in-plane electron-hole displacement vector, a_B is the exciton Bohr radius, and $f_{e(h)}(z)$ are the electron (hole) envelope functions in the growth direction, the superposition integrals read,

$$I^{\parallel}_{e(h)}(|\mathbf{q}|) = \left[1 + \left(\frac{m_{h(e)}}{2M} |\mathbf{q}| a_B \right)^2 \right]^{-3/2}, \tag{5a}$$

$$I^{\perp}_{e(h)}(q_z) = \int dz |f_{e(h)}(z)|^2 e^{i q_z z}. \tag{5b}$$

These integrals introduce cutoffs in the term $G(\mathbf{q}, q_z)$ for $|\mathbf{q}| > 1/a_B$, and for $q_z > 2\pi/L_{\text{QW}}$, where L_{QW} is the QW width. The latter cutoff originates from the electron and hole localization in the QW region described by the envelope functions $f_{e(h)}(z)$. This dependence of the cutoff in $I^{\perp}_{e(h)}(q_z)$ on L_{QW} indicates that the exciton-phonon interaction decreases for larger QW's. This cutoff becomes critical for small QW's. In this case, the penetration in the barriers of the exciton wave function has to be correctly included in $f_{e(h)}(z)$, otherwise the scattering rates are going to be overestimated. The intraband transition rate for excitons scattered by acoustic phonons is calculated by the Fermi golden rule. For instance, we obtain, in the case of transitions involving absorption of a phonon,

$$W^{\rm abs}_{\mathbf{k}\to\mathbf{k}'}=\frac{2\pi}{\hbar}\sum_{q_z}\ |\langle\mathbf{k}'|\langle n_{\mathbf{q},q_z}|H_{\rm exc\text{-}ph}|n_{\mathbf{q},q_z}+1\rangle|\mathbf{k}\rangle|^2 \times\delta[E_{\rm exc}(\mathbf{k}')-E_{\rm exc}(\mathbf{k})-E_{\rm ph}(\mathbf{q},q_z)]. \quad (6)$$

Here, $|\mathbf{k}\rangle$, $|\mathbf{k}'\rangle$ are the initial and final exciton states, and $|n_{\mathbf{q},q_z}\rangle$, $|n_{\mathbf{q},q_z}+1\rangle$ are the initial and final phonon states. $E_{\rm exc}(\mathbf{k})$, and $E_{\rm ph}(\mathbf{q},q_z)=\hbar u(|\mathbf{q}|^2+q_z^2)^{1/2}$, are the exciton and phonon energies, respectively. The rate $W^{\rm abs}_{\mathbf{k}\to\mathbf{k}'}$ is then averaged over the whole phonon ensemble, which is assumed to be in thermal equilibrium (phonon bath). Since the in-plane wave vector is conserved in the interaction, only phonons having $\mathbf{q}=\mathbf{k}'-\mathbf{k}$ contribute to the ensemble average. The sum over q_z may be performed exactly in the continuum limit, because of the δ function in Eq. (6). We finally obtain

$$W^{\rm abs}_{\mathbf{k}\to\mathbf{k}'}=\frac{4\pi}{\hbar}\frac{L_z}{2\pi}\frac{\hbar}{2\rho V}\frac{[|\mathbf{k}-\mathbf{k}'|^2+(q_z^0(\theta))^2]}{|\hbar u q_z^0(\theta)|} \times[a_e I_e^{\parallel}(|\mathbf{k}'-\mathbf{k}|)I_e^{\perp}(q_z^0)-a_h I_h^{\parallel}(|\mathbf{k}'-\mathbf{k}|)I_h^{\perp}(q_z^0)]^2 \times n_{\rm ph}[E_{\rm exc}(\mathbf{k}')-E_{\rm exc}(\mathbf{k})], \quad (7)$$

where q_z^0 is the root of the argument of the δ function

$$q_z^0=\left[\left(\frac{E(\mathbf{k}')-E(\mathbf{k})}{\hbar u}\right)^2-|\mathbf{k}-\mathbf{k}'|^2\right]^{1/2}, \quad (8)$$

and $n_{\rm ph}(E)$ is the Bose distribution function of the phonon population. We notice that $W^{\rm abs}_{\mathbf{k}\to\mathbf{k}'}$ depends only on $|\mathbf{k}|$, $|\mathbf{k}'|$, and the relative angle θ, because the interaction is isotropic. We remark that solutions of Eq. (8) do not exist for arbitrary values of $|\mathbf{k}|$, $|\mathbf{k}'|$, and θ. Equation (8) defines a phase space for the scattering process. The transitions assisted by phonon emission are calculated in a similar way, and contain a term $(n_{\rm ph}+1)$ instead of $n_{\rm ph}$.

In the QW, a 2D exciton with in-plane wave vector $\mathbf{k}$ interacts with photons having the same in plane wave vector, but with all possible values of k_z. Thus we have a density of states for the radiative decay,[1]

$$\rho(|\mathbf{k}|,\omega)=\sum_{k_z}\ \delta\left(E(\mathbf{k})-\hbar\frac{c}{n}\sqrt{|\mathbf{k}|^2+k_z^2}\right) =\frac{L_z}{2\pi}\frac{n}{\hbar c}\frac{2k_0}{\sqrt{k_0^2-|\mathbf{k}|^2}}\Theta(k_0-|\mathbf{k}|), \quad (9)$$

where k_0 is $n\omega_{\rm exc}/c$, and n is the refraction index. The function $\Theta(k)$ is the Heaviside function. We remark that the radiative recombination occurs only for states with $|\mathbf{k}|<k_0$. This defines the radiative zone. The radiative recombination rate for transverse excitons with a given $\mathbf{k}$ is calculated by the Fermi golden rule, using the exciton-photon interaction Hamiltonian,[1] and reads

$$\Gamma^T_{\mathbf{k}}=\frac{2\pi}{n}\frac{e^2}{m_0 c}\frac{f_{xy}}{S}\frac{k_0}{k_z}, \quad (10)$$

where f_{xy}/S is the oscillator strength per unit surface for transverse excitons, and $k_z=\sqrt{k_0^2-|\mathbf{k}|^2}$. For longitudinal excitons a factor k_z/k_0 replaces k_0/k_z in Eq. (10).

III. EVOLUTION OF THE DISTRIBUTION FUNCTION

The rate equations for the population $n_{\mathbf{k}}$ at a given in-plane $\mathbf{k}$, using the scattering rates $W_{\mathbf{k}\to\mathbf{k}'}$ and the radiative recombination rate $\Gamma_{\mathbf{k}}$ calculated in the previous section, read

$$\dot{n}_{\mathbf{k}}=\sum_{\mathbf{k}'}\ W_{\mathbf{k}'\to\mathbf{k}}n_{\mathbf{k}'}(n_{\mathbf{k}}+1)-\sum_{\mathbf{k}'}\ W_{\mathbf{k}\to\mathbf{k}'}n_{\mathbf{k}}(n_{\mathbf{k}'}+1)-\Gamma_{\mathbf{k}}n_{\mathbf{k}}. \quad (11)$$

The terms $(n_{\mathbf{k}}+1)$ are related to the bosonic character of excitons, and correspond to stimulated emission and absorption processes in the dynamics. However, at low exciton densities, when $n_{\mathbf{k}}\ll 1$, their contribution is negligible. We average the recombination rate in the whole radiative region in order to eliminate the infrared divergence of $\Gamma_{\mathbf{k}}$. We obtain

$$\langle\Gamma^T_{\mathbf{k}}\rangle=\frac{2\Gamma_0}{\Delta\mathbf{k}_{\rm rad}}\int_{\rm rad}\frac{k_0}{k_z}d\mathbf{k}=4\Gamma_0, \quad (12a)$$

$$\langle\Gamma^L_{\mathbf{k}}\rangle=\frac{2\Gamma_0}{\Delta\mathbf{k}_{\rm rad}}\int_{\rm rad}\frac{k_z}{k_0}d\mathbf{k}=\frac{4}{3}\Gamma_0, \quad (12b)$$

where $\Gamma_0=(\pi e^2/nm_0c)(f_{xy}/S)$, $\Delta\mathbf{k}_{\rm rad}$ is the area of the radiative zone in the $\mathbf{k}$ space, and L and T indicate longitudinal and transverse excitons, respectively. Assuming an initial isotropic distribution and taking into account that $W_{\mathbf{k}\to\mathbf{k}'}$ depends only on $|\mathbf{k}|$, $|\mathbf{k}'|$, and the angle θ between them, one readily sees that the distribution remains isotropic for all times. All the exciton parameters as Bohr radius, binding energies, oscillator strengths, masses etc., are taken from theoretical calculations.[11] We solve the Eq. (11) by direct numerical integration, using a grid of 800 $|\mathbf{k}|$ points in the region from 0 up to $20k_0$. We recall that exciton dissociation process has been neglected in our model. We study the dynamics of a realistic QW system of GaAs with $Ga_{0.6}Al_{0.4}As$ barriers and QW width of 40 Å. We also use $m_e=0.067m_0$ for the electron mass, and $m_h=0.18m_0$ for the heavy hole (m_0 is the free electron mass). In this system, the averaged radiative lifetimes are 4 ps and 12 ps for transverse and longitudinal excitons, respectively. In order to give a rough estimation of the characteristic times coming into play in the phonon scattering, we calculate the total rate of absorption for the excitons at $\mathbf{k}=0$. We obtain a typical absorption rate $R_{\rm abs}=\gamma T$, with $\gamma=4\ \mu$eV/K. This compares well with degenerate four wave mixing and photoluminescence linewidth measurements.[12–14] Larger absorption rates are found for excitons with $\mathbf{k}\neq 0$, because of additional phonon emission processes and because of a wider scattering phase space. Once all the rates $W_{\mathbf{k}\to\mathbf{k}'}$, Γ_0, and the initial distribution $n_{\mathbf{k}}(0)$ are known, the rate equations can be numerically integrated to obtain the time dependence of $n_{\mathbf{k}}$. The luminescence signal is easily extracted, because it is proportional to the total number of photons emitted in the whole solid angle per unit time,

$$I_{\rm PL}(t)\propto\sum_{|\mathbf{k}|\le k_0}\Gamma_{\mathbf{k}}n_{\mathbf{k}}(t). \quad (13)$$

In Figs. 1(a) and (b), we show the solution $n_{\mathbf{k}}(t)$ of Eq. (11) at different times after the nonresonant excitation as a func-

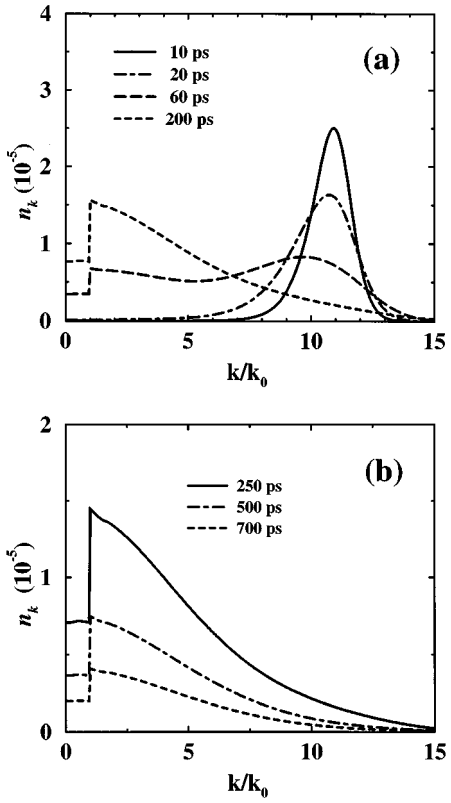

FIG. 1. Time evolution of the exciton population $n_{\mathbf{k}}$ at $T=50$ K. The QW width is 40 Å . (a) Evolution up to 200 ps. (b) Evolution after 250 ps.

tion of **k**. The initial exciton population created with an excess energy cools down by emission of phonons. In this first part of the evolution, shown in Fig. 1(a), the total number of excitons in the radiative zone increases and the PL intensity, shown in Fig. 2, correspondingly rises. The exciton distribution subsequently tries to thermalize to the lattice temperature, but the coupling with photons drains the excitons away from the radiative zone, preventing full thermalization of the excitonic population. We see indeed that the exciton distribution is depleted in the radiative region. Afterwards, the population maintains a stationary shape and rigidly decreases in time, as shown in Fig. 1(b), so that it may be parametrized

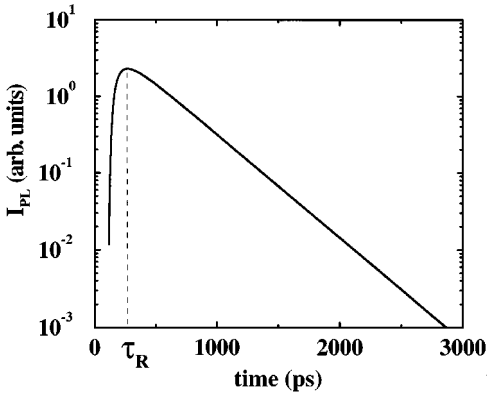

FIG. 2. Photoluminescence signal as a function of time for nonresonant excitation. Same parameters as in Fig. 1. The rise time of the signal is indicated by τ_R.

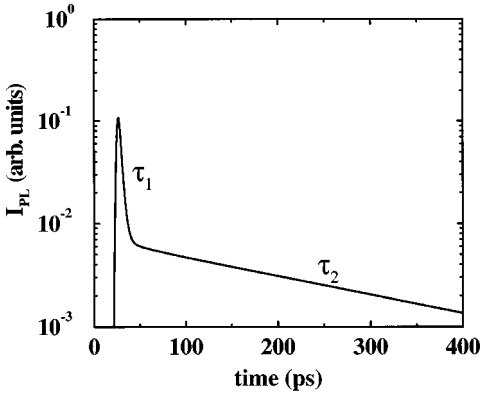

FIG. 3. Photoluminescence signal as a function of time for resonant excitation of the $\mathbf{k}=0$ excitons. The temperature is 10 K. $\tau_1=4$ ps and $\tau_2=240$ ps are the two decay times introduced in the text.

as $n_{\mathbf{k}}(t)=f_{\mathbf{k}}^{\mathrm{stat}}N_{\mathrm{tot}}(t)$. The total population, the radiative population, and the PL intensity, therefore, decay with the same characteristic time τ_D. This decay time may be calculated by summing Eq. (11) over **k**,

$$-\frac{\dot{N}_{\mathrm{tot}}}{N_{\mathrm{tot}}}=\frac{1}{\tau_D}=\frac{\Sigma_{|\mathbf{k}|\leqslant k_0}\Gamma_{\mathbf{k}}n_{\mathbf{k}}}{\Sigma_{\mathbf{k}}n_{\mathbf{k}}}=\sum_{|\mathbf{k}|\leqslant k_0}f_{\mathbf{k}}^{\mathrm{stat}}\Gamma_{\mathbf{k}}. \qquad (14)$$

We observe that τ_D depends on the fraction of excitons in the radiative region only.

When the sample is resonantly excited, we have an initial exciton population peaked at $\mathbf{k}=0$. A different profile of the PL signal, with respect to the nonresonant case is thus produced, as shown in Fig. 3. In this case the PL shows two decay times. The initial decay time τ_1 corresponds to the recombination of excitons before the stationarity of the normalized distribution function is reached. This first time is related to both the radiative recombination rate Γ_0 and the phonon scattering rate from the initial exciton state to all the other exciton states. It, therefore, shows a weak temperature dependence. The second decay time appears after about 30 ps, when the same stationary distribution as in the nonresonant excitation case is reached. This decay time τ_2 is, therefore, the same as in the nonresonant excitation case, τ_D. The presence of the two characteristic decay times in the case of resonant excitation has been observed experimentally by Deveaud *et al.*[15] The main limitation of our model consists in the assumption that the optically excited states lose their coherence in a time much shorter than the relaxation time of the exciton population. Actually, this assumption is well justified in the case of nonresonant excitation, where the relaxation of the hot carriers destroy the coherence. However, it does not hold in the case of direct excitation of the excitons. Thus, our model provides only a partial understanding of the evolution in this resonant case. Several measurements have been performed in the quasiresonant excitation regime[6,15] (a few meV above the bottom of the HH exciton band). We remark that our model does not cover this regime.

IV. TEMPERATURE DEPENDENCE OF THE CHARACTERISTIC TIMES

We show, in Fig. 4, the temperature dependence of the rise time in the case of nonresonant excitation. Energy relax-

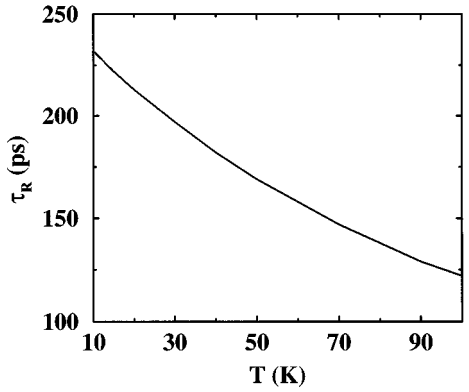

FIG. 4. Temperature dependence of the rise time τ_R for nonresonant excitation.

ation of the initial exciton distribution is provided by the phonon emission process. Therefore, the rise time shortens with increasing temperature, because larger phonon densities at higher temperatures produce faster exciton cooling. A comparison of the temperature dependence of the rise time with experimental data provides a significant test for the reliability of the calculated phonon scattering rates. Measurements of the rise time in good quality samples have been reported by many groups,[4–6,16] and compare reasonably well to the values found in the present calculation for excitation energy far from the LH exciton level. We have verified that the shape of the initial distribution function modifies the dynamics. In particular, the value of the rise time is directly related to the position of the maximum of this initial distribution. Furthermore, we have found that the computed rise times are very sensitive to the values of the parameters appearing in the exciton-phonon interaction. In particular, a small change in the absolute values of the deformation potentials changes the rise times considerably. We recall that the relative deformation potential (i.e., $a_e - a_h$) can be measured directly by applying hydrostatic pressure on the samples,[8] but for the absolute values a_e, and a_h, only indirect measurements[9] or theoretical estimations are available.[17] We have considered, in our calculation, several values for the deformation potentials. We have found that the results on the quasithermalization of the exciton states still hold, and the values of the decay times do not change in an appreciable way.

In Fig. 5, we give the temperature dependence of the decay times for transverse excitons. The corresponding dependence resulting from the assumption of full thermalization is also shown. The decay times are underestimated by the full thermalization picture, but the thermal slope is recovered at high temperatures, as indicated by the guideline in Fig. 5. This behavior can be explained by considering the role of the deviations from the thermal distribution. In fact, we observe that the stationary shape $f_{\mathbf{k}}^{\mathrm{stat}}$ differs from the thermal distribution mainly in the radiative region. This means, according to Eq. (14), that recombination rates obtained by averaging over the distribution $f_{\mathbf{k}}^{\mathrm{stat}}$ become smaller. We show in Fig. 6 two stationary distribution functions at different temperatures. The deviations are smaller at higher temperature, but do not vanish. Let us discuss in detail the role of these deviations. We write the population $n_{\mathbf{k}}$ as

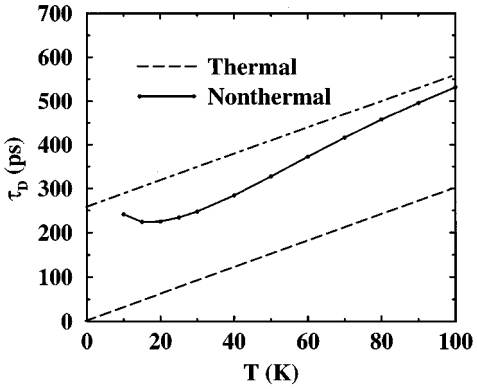

FIG. 5. Temperature dependence of the photoluminescence decay time τ_D for a QW of 40 Å . The dashed line represents the full thermalization case. The dot-dashed line is a guideline parallel to the previous one.

$$n_{\mathbf{k}} = N_{\mathrm{tot}}(t) f_{\mathbf{k}}^{\mathrm{stat}} = N_{\mathrm{tot}} f_{\mathbf{k}}^{0} - \delta n_{\mathbf{k}}, \tag{15}$$

where $f_{\mathbf{k}}^{0}$ is the Boltzmann distribution and $\delta n_{\mathbf{k}}$ represents the deviations. We have $\Sigma_{\mathbf{k}} \delta n_{\mathbf{k}} = 0$, because distribution functions are normalized. Using the detailed balance principle,

$$W_{\mathbf{k}' \to \mathbf{k}} f_{\mathbf{k}}^{0} - W_{\mathbf{k} \to \mathbf{k}'} f_{\mathbf{k}'}^{0} = 0, \tag{16}$$

holding for all $\mathbf{k}$ and $\mathbf{k}'$, and inserting Eq. (15) into Eq. (11), we obtain

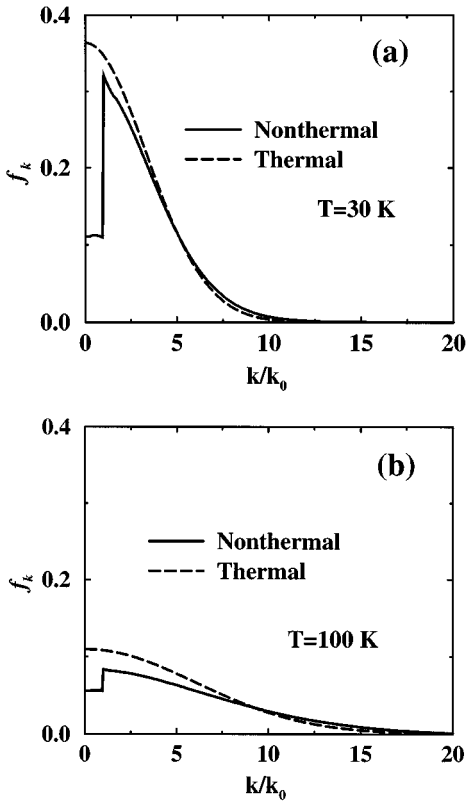

FIG. 6. Normalized exciton distribution functions $f_{\mathbf{k}}^{\mathrm{stat}}$, for two different temperatures, 700 ps after the excitation. The dashed lines show the thermal distributions corresponding to the same temperatures.

$$\dot{n}_{\mathbf{k}} = -\sum_{\mathbf{k}'} W_{\mathbf{k}'\to\mathbf{k}}\delta n_{\mathbf{k}'} + \sum_{\mathbf{k}'} W_{\mathbf{k}\to\mathbf{k}'}\delta n_{\mathbf{k}} - \Gamma_{\mathbf{k}} n_{\mathbf{k}}. \quad (17)$$

In deducing Eq. (17) from Eq. (11), we have assumed $n_{\mathbf{k}} \ll 1$ and we have neglected all the $(n_{\mathbf{k}}+1)$ terms. We now introduce a simplified model in order to analyze the role of the deviations from the thermal distribution. For this purpose, we define two effective levels, which represent the totality of radiative and nonradiative excitons, respectively. We will indicate the quantities related to the radiative and nonradiative regions with indexes R and NR, respectively. We first consider the behavior of the total nonradiative population $N_{\mathrm{NR}}(t)$. Summing Eq. (17) over $|\mathbf{k}_{\mathrm{NR}}|$ in the nonradiative zone, we obtain

$$\dot{N}_{\mathrm{NR}}(t) = \sum_{\mathbf{k}_{\mathrm{NR}}} \sum_{\mathbf{k}'_R} (-W_{\mathbf{k}'_R\to\mathbf{k}_{\mathrm{NR}}}\delta n_{\mathbf{k}'_R} + W_{\mathbf{k}_{\mathrm{NR}}\to\mathbf{k}'_R}\delta n_{\mathbf{k}_{\mathrm{NR}}}). \quad (18)$$

Clearly, the scattering inside the nonradiative zone does not modify $N_{\mathrm{NR}}(t)$. Therefore, in Eq. (18), we consider only exchanges between nonradiative and radiative zones. We define the total exchange rates as

$$W_{R\to\mathrm{NR}}(\mathbf{k}'_R) = \sum_{\mathbf{k}_{\mathrm{NR}}} W_{\mathbf{k}'_R\to\mathbf{k}_{\mathrm{NR}}}, \quad (19)$$

$$W_{\mathrm{NR}\to R}(\mathbf{k}_{\mathrm{NR}}) = \sum_{\mathbf{k}'_R} W_{\mathbf{k}_{\mathrm{NR}}\to\mathbf{k}'_R}. \quad (20)$$

These rates are flat functions of $\mathbf{k}$, where the deviation $\delta n_{\mathbf{k}}$ are large. We rewrite Eq. (18) as

$$\dot{N}_{\mathrm{NR}}(t) = -W\delta N_R, \quad (21)$$

where we have defined $\delta N_R = \Sigma_{\mathbf{k}_R}\delta n_{\mathbf{k}_R} = -\delta N_{\mathrm{NR}} = -\Sigma_{\mathbf{k}_{\mathrm{NR}}}\delta n_{\mathbf{k}_{\mathrm{NR}}}$ and $W = W_{R\to\mathrm{NR}} + W_{\mathrm{NR}\to R}$. Analogously, by summing Eq. (11) over the radiative states, we obtain

$$\dot{N}_R(t) = W\delta N_R - \Gamma N_R. \quad (22)$$

Equation (21) shows that a transfer of excitons from the nonradiative to the radiative region is generated by the deviation δN_R. In the stationary regime, all the excitons decay with the same characteristic time, thus

$$\frac{\dot{N}_R}{N_R} = \frac{\dot{N}_{\mathrm{NR}}}{N_{\mathrm{NR}}} = \frac{\dot{N}_{\mathrm{tot}}}{N_{\mathrm{tot}}}, \quad (23)$$

and, recalling that $N_{\mathrm{tot}} = N_R + N_{\mathrm{NR}}$, we obtain from Eqs. (21) and (22),

$$\Gamma\frac{N_R}{N_{\mathrm{tot}}} = \Gamma - W\frac{\delta N_R}{N_R}. \quad (24)$$

Summing Eq. (15) over the radiative region, we write

$$N_R = \sum_{\mathbf{k}_R} n_{\mathbf{k}} = \alpha N_{\mathrm{tot}} - \delta N_R, \quad (25)$$

where $\alpha = \Sigma_{\mathbf{k}_R} f^0_{\mathbf{k}} = 1 - e^{-E_1/(k_B T)}$, and $E_1 = (\hbar k_0)^2/(2M)$. Introducing Eq. (25) into Eq. (24), we finally obtain

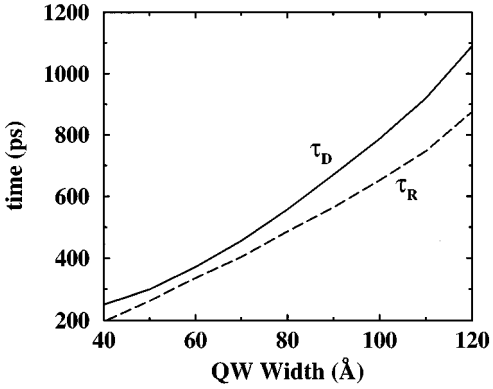

FIG. 7. Quantum-well width dependence of decay and rise times. The temperature is 30 K.

$$\alpha\Gamma\left(1 - \frac{\delta N_R}{\alpha N_{\mathrm{tot}}}\right) = \Gamma - W\frac{\delta N_R}{\alpha N_{\mathrm{tot}}}\left(1 - \frac{\delta N_R}{\alpha N_{\mathrm{tot}}}\right)^{-1}. \quad (26)$$

For $W(T) \gg \Gamma$, we obtain from Eq. (26) that $\delta N_R/(\alpha N_{\mathrm{tot}}) \ll 1$. In this case, the full thermalization limit is reached. This limit holds for high temperatures, because $W(T)$ is an increasing function of temperature. In this limit, to the first order in $\delta N_R/(\alpha N_{\mathrm{tot}})$ in Eq. (26), we obtain

$$\frac{\delta N_R}{\alpha N_{\mathrm{tot}}} \simeq \frac{\Gamma}{W}. \quad (27)$$

We calculate the temperature dependence of $W(T)$ from Eqs. (19) and (20), and we find $W(T) = \gamma T$, with $\gamma = 4$ μeV/K. For transverse excitons in a QW of 40 Å with $\langle\Gamma^T_{\mathbf{k}}\rangle = 185$ μeV, the condition $\delta N_R/(\alpha N_T) \ll 1$ holds for $T \gg$ 50 K. In this limit

$$\tau_D(T) = \left[\frac{\Gamma E_1}{k_B T}\left(1 - \frac{\Gamma}{W}\right)\right]^{-1} \simeq \frac{k_B T}{\Gamma E_1} + \frac{k_B}{\gamma E_1}, \quad (28)$$

where we have used $\alpha \simeq E_1/(k_B T)$, which holds for T $\gg$ 1 K. At high temperature, $\tau_D(T)$ increases with a slope $(k_B)/(4\Gamma_0 E_1) =$ 3.0 ps/K for transverse excitons as predicted in the full thermalization limit. In addition, we find an offset $k_B/(\gamma E_1) =$ 150 ps. Comparison of this latter result to the calculated $\tau_D(T)$ given in Fig. 5 shows that our simplified model slightly underestimates this offset. This fact may be due to the assumption of a $\mathbf{k}$ independent $W(\mathbf{k})$. Concerning comparison of the calculated value of the offset of $\tau_D(T)$, it should be kept in mind that trapping of excitons at interfaces of real samples contributes to the observed offset.[2]

The deviations from a thermal distribution are found also in the case of continuous wave (cw) nonresonant excitation luminescence. The shape of the distribution function, which is stationary in this case, is very similar to the $f^{\mathrm{stat}}_{\mathbf{k}}$ shown in Fig. 6. We therefore remark that, also in this cw case, evidence of this departure from the thermal distribution can only be indirectly deduced.

Finally, we study the characteristic times of the PL as a function of the well width. We show in Fig. 7 the dependence of both decay and rise times on the QW width. These times increase with the well width. For decay times, this is mainly due to the reduction of the oscillator strength f_{xy}/S

[see Eq. (10)], due to the less effective exciton confinement. The behavior of the rise times is related to the well width dependence of the cutoff in the exciton-phonon interaction, as discussed in Sec. II. In fact, the superposition integral $I^{\perp}_{e(h)}(q_z)$ of the phonon wave function with the exciton envelope function in the growth direction is a decreasing function of the well width. This behavior of the rise time as a function of the well width has been experimentally observed.[18] However, in Ref. 18, the temperatures are too large to be addressed by our model. Experiments at lower temperatures are, therefore, needed in order to have an independent check of the parameters used in the exciton-phonon interaction.

V. THE ROLE OF THE SPIN

Up to now, we have only considered the dynamics of transverse excitons. Actually, there are four HH exciton levels: one longitudinal, and one transverse, which correspond to the Γ_5 representation of the T_d point group, and two dark excitons, the states of which belong to the representation Γ_1 and Γ_2. The dark excitons do not couple with the light. We have not extended our model in order to take into account the scattering between these levels. We only make here some considerations about the role of this scattering on the overall dynamics of excitons.

The first possibility is that scattering between the four levels is absent, or at least it is much slower than phonon scattering and recombination characteristic times. It follows from this assumption that in the dynamics we have four parallel channels, and the PL signal results from the sum of the PL produced by longitudinal and transverse excitons. Therefore one expects to observe, for sufficiently large times, a sum of two exponential decays in the signal. Furthermore, the total PL signal depends on the ratio of longitudinal to transverse excitons created at the beginning. The two decay times as a function of the temperature corresponding to longitudinal and transverse excitons are reported in Fig. 8(a).

The second possibility is that the scattering rates between the optically active excitons and the dark excitons are negligible, and the scattering rate between the two optically active states is faster than the radiative recombination rates. As a consequence, the populations of longitudinal and transverse excitons are equal. Therefore, the averaged radiative recombination rate is

$$\langle \Gamma \rangle = \frac{\langle \Gamma^L_{\mathbf{k}} \rangle + \langle \Gamma^T_{\mathbf{k}} \rangle}{2}. \tag{29}$$

We show in Fig. 8(b) the decay time $\tau_D(T)$ corresponding to this assumption.

The last possibility is that a fast scattering involves all the four levels. In this case, we also need a scattering mechanism between optically active excitons ($J = \pm 1$) and dark excitons ($J = \pm 2$). This could be provided by a spin flip of the electron as in the D'yakonov-Perel[19] or Elliott-Yafet[20] mechanism, or by spin flip of the hole.[21] Inserting into the rate equation the averaged radiative rate over the four levels,

$$\langle \Gamma \rangle = \frac{\langle \Gamma^L_{\mathbf{k}} \rangle + \langle \Gamma^T_{\mathbf{k}} \rangle}{4}, \tag{30}$$

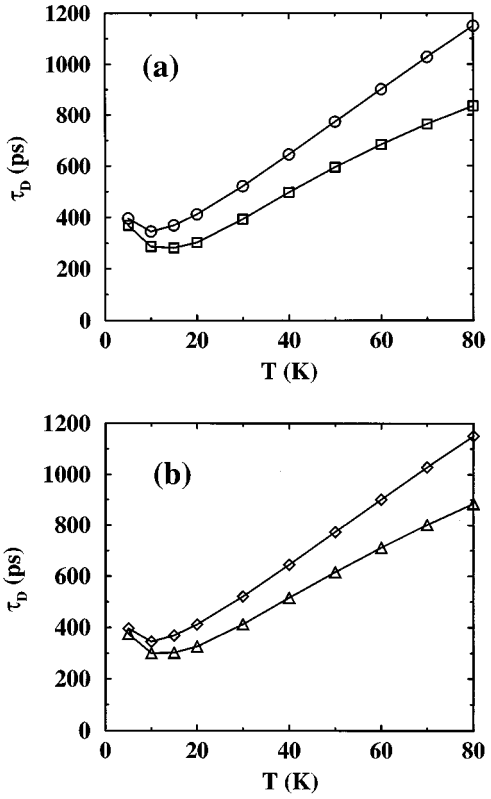

FIG. 8. Temperature dependence of τ_D for a QW of 50 Å corresponding to the following cases. (a) no scattering between different exciton spin levels: transverse excitons (squares), and longitudinal excitons (circles); (b) fast scattering rate between the two optically active states (triangles), fast scattering rates between all the four exciton spin levels (diamonds).

we calculate the corresponding dynamics in this case. Results are shown again in Fig. 8(b). Fitting procedures from polarized resonant PL experiments give some estimations of the typical relaxation rates between the spin levels. Vinattieri *et al.*[22] have shown that, for a QW of 150 Å at 12 K, the scattering time between optical states is 70 ps, the hole spin-flip time is 100 ps, while the electron spin-flip time ranges between 300 ps and 3 ns. These values suggest that the first possibility in our discussion is presumably the most reliable. Theoretical models for the understanding of the relaxation mechanisms and the estimation of these times have been proposed by Maialle *et al.*[23] However, an essential improvement to these theories is necessary in order to include explicitly the interaction with the phonons, and to produce quantitative results in a full analysis of the relaxation processes similar to the one proposed in this paper.

VI. CONCLUSIONS

We have shown that, in the free exciton dynamics in QW's, there is a competition between the phonon scattering and radiative recombination. This led us to relax the hypothesis of a thermal distribution for excitons while they are recombining. A rate equation model has been introduced, where scattering by acoustic phonons has been taken into account. A depletion of the radiative zone resulted from our calculation. A signature of this depletion can be observed in

the temperature dependence of the PL decay times in good quality samples, where only free excitons are created. In particular, we have predicted a finite PL decay time at low temperature, which is much larger than the intrinsic one, and a linear increase at higher temperature with the same slope as in the limit of full thermalization, but with an offset which is typically 200 ps for a QW of 40 Å . The results are very sensitive to the physical parameters used in the calculation like the deformation potentials and the masses of the carriers. Detailed comparison with the experimental measurements of the characteristic times would result in an assessment of the values to be used. We have also indicated that spin relaxation has a fundamental role in the PL dynamics, because two radiative and two dark states exist. We have produced typical results expected in limit situations of very slow or very fast spin relaxation. The inclusion of intermediate cases is part of future research.

ACKNOWLEDGMENTS

C.P. acknowledges support by the Swiss National Science Foundation and F.T. acknowledges support by the Swiss National Priority Program for Optics. We are grateful to L. C. Andreani and to B. Deveaud for many useful discussions and suggestions.

[1] L. C. Andreani, F. Tassone, and F. Bassani, Solid State Commun. **77**, 641 (1991).
[2] D. S. Citrin, Phys. Rev. B **47**, 3832 (1993).
[3] J. Feldmann, G. Peter, E. O. Göbel, P. Dawson, K. Moore, C. Foxon, and R. J. Elliott, Phys. Rev. Lett. **59**, 2337 (1987).
[4] J. Martinez-Pastor, A. Vinattieri, L. Carraresi, M. Colocci, Ph. Roussignol, and G. Weimann, Phys. Rev. B **47**, 10 456 (1993).
[5] T. C. Damen, Jagdeep Shah, D. Y. Oberli, D. S. Chemla, J. E. Cunningham, and J. M. Kuo, Phys. Rev. B **42**, 7434 (1990).
[6] Ph. Roussignol, C. Delalande, A. Vinattieri, L. Carraresi, and M. Colocci, Phys. Rev. B **45**, 6965 (1992).
[7] See, for instance, *Hot Carriers in Semiconductor Nanostructures: Physics and Applications*, edited by Jagdeep Shah (Academic Press, Boston, 1992).
[8] C. M. Wolfe, G. E. Stilman, and W. T. Lindley, J. Appl. Phys. **41**, 3088 (1970).
[9] S. Lee, J. Sanchez-Dehesa, and J. D. Dow, Phys. Rev. B **32**, 1152 (1985).
[10] H. Stolz, D. Schwarze, W. van der Osten, and G. Weimann, Superlatt. Microstruct. **6**, 271 (1989).
[11] L. C. Andreani and A. Pasquarello, Phys. Rev. B **42**, 8928 (1990); L. C. Andreani, Ph.D. thesis, Scuola Normale Superiore, Pisa, 1989.
[12] L. Schultheis, A. Honold, J. Kuhl, K. Köhler, and C. W. Tu, Phys. Rev. B **34**, 9027 (1986).
[13] Dai-Sik Kim, Jagdeep Shah, J. E. Cunningham, T. C. Damen, Wilfried Shäfer, Michael Hartmann, and Stefan Schmitt-Rink, Phys. Rev. Lett. **68**, 1006 (1992).
[14] D. Gammon, S. Roudin, T. L. Reinecke, D. S. Katzer, and C. S. Kyono, Phys. Rev. B **51**, 16 785 (1995).
[15] B. Deveaud, F. Clérot, N. Roy, K. Satzke, B. Sermage, and D. S. Katzer, Phys. Rev. Lett. **67**, 2355 (1991); B. Deveaud, F. Clérot, B. Sermage, C. Dumas, and D. S. Katzer, in *Optical Phenomena in Semiconductor Structures of Reduced Dimension*, edited by D. J. Loockwood and A. Pinczuk (Kluwer Academic, Dordrecht, 1993).
[16] X. Marie, F. Lephay, T. Amand, J. Barrau, F. Voillot, and M. Brosseau, Superlatt. Microstruct. **10**, 415 (1991).
[17] *Physics of Group IV Elements and III-V Compounds* , edited by A. M. Hellwege and O. Madelung, Landolt-Börnstein, New Series, Group III, Vol. 17, Pt. a (Springer-Verlag, Berlin, 1982).
[18] T. Furuta, M. Tomizawa, and A. Yoshii, J. Appl. Phys. **78**, 596 (1995)
[19] M. I. D'yakonov and V. I. Perel, Zh. Éksp. Teor. Fiz. **60**, 1954 (1971) [Sov. Phys. JETP **33**, 1053 (1971)].
[20] R. J. Elliott, Phys. Rev. **96**, 266 (1954).
[21] T. Uenoyama and L. J. Sham, Phys. Rev. Lett. **64**, 3070 (1990).
[22] A. Vinattieri, Jagdeep Shah, T. C. Damen, D. S. Kim, L. N. Pfeiffer, M. Z. Maialle, and L. J. Sham, Phys. Rev. B **50**, 10 868 (1994).
[23] M. Z. Maialle, E. A. de Andrada e Silva, and L. J. Sham, Phys. Rev. B **47**, 15 776 (1993).